Journal of Ceramic Processing Research. Vol. 3, No. 3, pp. 210~215 (2002)

J O U R N A L O F
Ceramic Processing Research

Effects of the plasma gas composition on the coating formation and coating properties of the APS Al_2O_3-TiO_2 coating

Hanshin Choi, Changhee Lee* and Hyungjun Kim[a]

Dept. of the Mater. Sci. and Eng., CPRC, Hanyang Univ., Seoul 133-791, Korea

[a]CAPST, Welding & Structural Integrity Research Team, RIST, Phohang 790-600, Korea

The effects of the plasma gas composition on the formations of the splat, the single passed spraying bea d, and the coating and the resultant coating properties were investigated using an Al_2O_3-13 wt.%TiO_2 commercial grade clad powder. The plasma gas consisted of the argon gas and the hydrogen gas. By controlling the plasma gas compositions in the atmospheric plasma spraying process, both particle velocity and enthalpy were designed to change under the constant feeding parameters, spray distance, cooling condition, and spray current. Splat morphology was examined using the scanning electron microscopy, and the effects of the plasma gas composition on the splashing degree were considered. The splashing degree of the splat was increased with the increases of the hydrogen gas flow rate and the argon gas flow rate. And also the chemistry of the impacting particle might affect the splashing behaviors. The geometries of the single passed spaying beads were evaluated by observing the plane-view morphology and the cross sectional morphology using the SEM and image analyzer. While the argon gas decreased the bead width and thickness, the bead width and thickness were increased with the increase of the hydrogen gas fraction in the plasma gas. In addition, the argon gas fraction increased the bead symmetry, which implies that the trajectories of the in-flight particles are largely dependent on the plasma gas composition. According to gas compositions, coating thickness, porosity, microhardness, and bond strength were measured. Cross-sectional coating morphologies were observed using SEM. Microharndess as well as coating thickness and porosity seemed to be dependent on the melting state of the in-flight particle largely affected by the enthalpy of the plasma jet stream. Meanwhile, the bond strength of coating depended on the velocity of the plasma jet affecting the particle impacting velocity and the contact interface properties. Thus, the coating properties were dependent on the plasma gas compositions and this means that the coating properties can be tailored by controlling the plasma gas compositions.

Key words: alumina-titania, splat formation, single passed spraying bead.

Introduction

The atmospheric plasma spraying process is one of the thermal spraying technologies for modifying the surface properties of the structural materials [1]. The ceramic materials can be applied for the overlay coating due to the higher gas enthalpy of the thermal plasma jet. The feedstock materials are vertically or axially injected into the hot gas stream. During the flight of the injected particle, it undergoes the heat and momentum transport reactions with the hot gas stream. Both reactions heat and accelerate the in-flight particles [2]. At the moment of the impaction onto the substrate surface or the previously deposited layer, it flattens and solidifies rapidly to form a splat. As the thermal spray coatings are produced by the build-ups of these splats, the splat morphology and deposition are very important. In fact, the splat morphology is affected by the impacting particle parameters such as particle temperature, particle velocity, and particle size [3, 4]. The coating properties are largely dependent on the coating microstructures including defect-like microstructures. Also the coating microstructures depend on the process parameters such as the impacting particle parameters and the substrate parameters. Therefore, the process should be optimized in order to improve the coating properties as required. However, there are so many processing parameters affecting the coating microstructures and coating properties. This requires the effective processing parameters.

In this study, the plasma jet properties were changed by changing the plasma gas composition with the viewpoint of the fact that the energy of an in-flight particle is primarily dependent on the plasma jet properties. As spraying power is the multiplication of enthalpy and total plasma gas mass flow rate, the enthalpy of the plasma jet can be different under the same spraying power according to the gas flow rate and gas composition. Therefore, the electrical power of a plasma jet was considered as the total energy of plasma jet, and the Ar flow fraction and H_2 flow fraction were used as the approximate kinetic energy factor and the thermal energy one, respectively as shown in Fig. 1.

*Corresponding author:
Tel : +82-2-2290-0388
Fax: +82-2-2290-1976
E-mail: chlee@hanyang.ac.kr

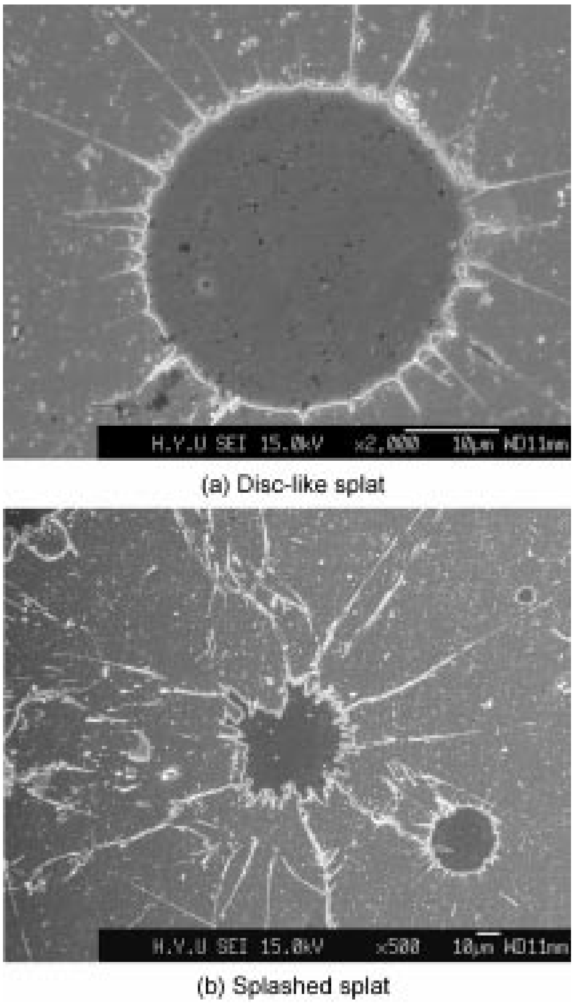

Fig. 1. Splat morphologies.

Through this approach, the coating properties were evaluated by changing the plasma gas compositions in order to vary the particle energy combination.

Experiments

The feedstock material was Metco 130 powder; 13 wt.% titania was cladded to alumina, and the particle size distribution was -53+15 μm. The combinations of the spraying parameters can be seen in Table 1. The evaluation of the plasma gas composition effects were divided into three parts; the splat formation, the single passed spraying bead formation, and the coating formation. In the case of the splat formation, the substrate was fine polished to the # 1000 SiC abrasive paper. And the feeding rate of the powder materials was 1 $gmin^{-1}$. STS (stainless steel) 304 substrates for the spraying bead formation and coating formation were grit blasted with SiC grit and then they were ultrasonically cleaned with acetone and alcohol. The plasma gas consisted of argon (1^{st} gas) and hydrogen (2^{nd} gas), and the arc current was fixed at the value of 500 A. Alumina-titania feedstock powder was injected into the plasma jet vertically at the feeding rate of 30 g m^{-1}. Metco 3MB plasma gun traveled at the speed of 500 mm s^{-1} horizontally. And the vertical step distance was 3.5 mm. A coating was deposited for 4 cycles. The coating thickness according to spraying parameters was measured using scanning electron microscopy (SEM) and an image analyzer. Vickers microhardness was measured on the normal to both the surface and the cross-section of coatings that had been finely polished down to the 1 μm diamond suspension. Indentation conditions were set to a 300 g-force for 15s for a single loading-unloading cycle, considering the indentation size effect (ISE) and coating geometry [5]. At least 20 points were measured for each specimen. Bond strength of the plasma sprayed coatings was measured by the Sebastian IV method. The stud diameter used was 1.5 mm. All the specimens were cut into 20*20 mm squares, and the surfaces were polished with no. 1000 SiC abrasive paper. After that, the specimens were ultrasonically cleaned using acetone and alcohol. The epoxy was cured in the oven fixed at 150ºC for 90 min. six samples were measured for each condition. Failed surface and cross-section were examined using SEM.

Table 1. Process parameters

Invariable parameters			
Plasma gas system	1^{st} gas	2^{nd} gas	Carrier gas
	Ar	H_2	Ar
	100 psi	50 psi	120 psi
Nozzle inlet diameter	6.5 mm		
Substrate pre-heating	1 cycle		
Spraying distance	65 mm		
Powder feeding rate	30 gm^{-1}		

Variable parameters	Notation	Ar	H_2	Total	H_2 ratio (vol.%)
Plasma gas flow rate (FMR)	AT1	100	20	120	16.7
	AT2	100	10	110	9.1
	AT3	80	20	100	20.0
	AT4	80	10	90	11.1

Results and Discussions

Splashed splats through disc-like splats could be all observed in this study, as shown in Fig. 1. Splashing degree of the impacting particle was dependent on the plasma gas composition. It was increased with the increases of the argon gas flow rate, the hydrogen gas flow rate and the particle size. In addition, it also depended on the particle parameters such as the chemical composition of the impacting particles and the particle size. Except the particle chemistry, the

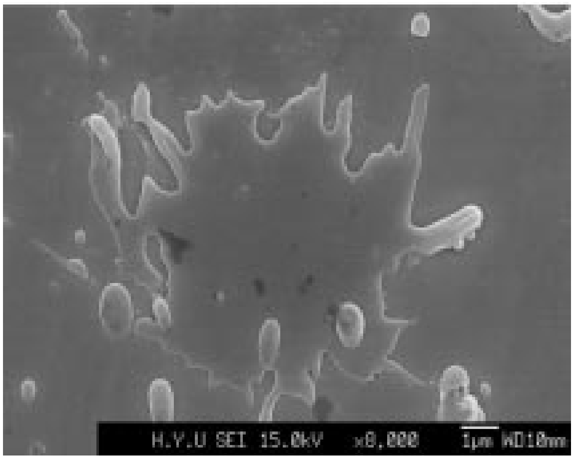

Fig. 2. Substrate melting.

effects of the other characteristics of the impacting particle on the inclination of the splashing could be interpreted with the viewpoint of the Taylor-Rayleigh instability [2]. In the case of the splats deposited using 20 H_2 FMR (AT1 and AT3), the substrate melting was observed at the surface after splat spallation as it can be seen in Fig. 2. From the plane view morphology of the substrate melting, the intimate contact between the substrate and impacting particle was limited at the initial impacting area and the jetting away of the spreading particle could be assumed. On the other hand, the substrate melting might improve the mechanical bonding property by enhancing the mechanical keying effect. The plasma gas composition effects on the geometry of the single pass spraying bead were examined. Figure 3(a) shows the plane view morphologies of the spraying beads according to the plasma gas composition. For

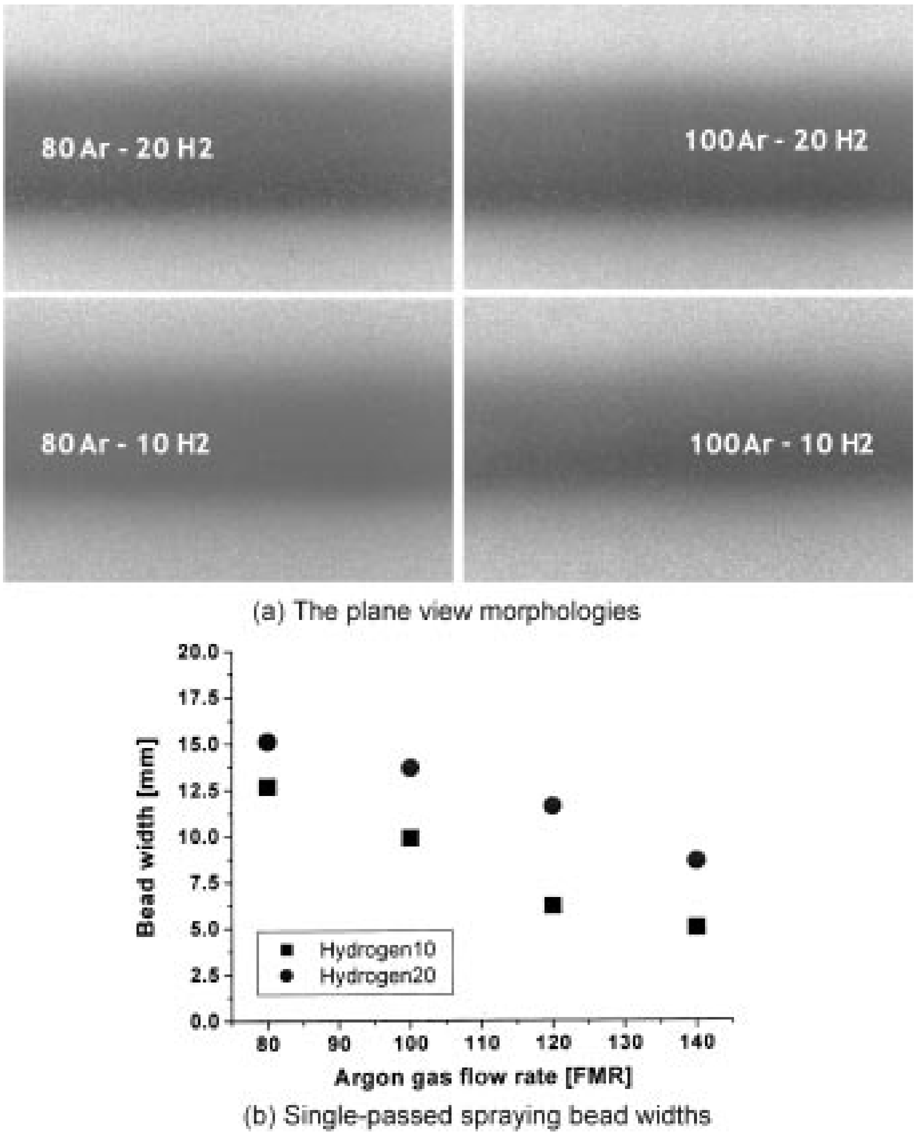

Fig. 3. Morphology and width of the single-passed spraying beads according to the plasma gas composition (See Table 1 for the plasma gas composition).

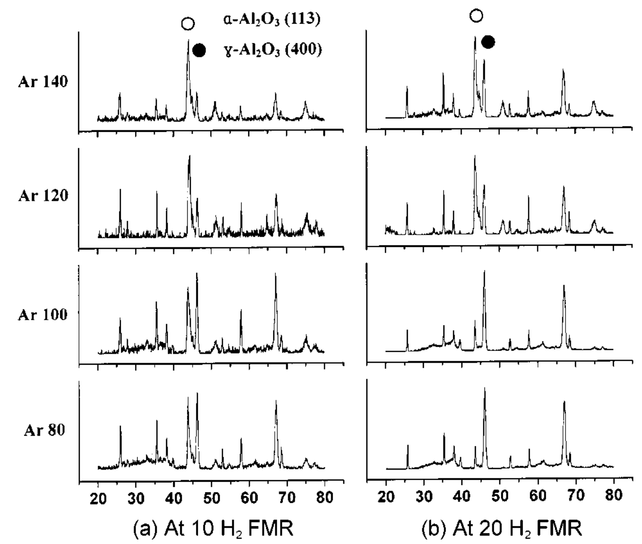

Fig. 4. Phase composition of the single-passed spraying bead.

comparison, other plasma gas compositions were considered. As the argon gas flow rate was increased, the width of the spraying bead was decreased. However, the width was increased with the increase of the hydrogen gas flow rate as shown in Fig. 3(b). In the case of the cross-sectional shapes of the spraying beads, the hydrogen gas increased the spraying bead thickness while the argon gas increased the symmetry of the spraying bead. Indirectly, the trajectories as well as the temperatures of the in-flight particles can be deduced through the spraying bead morphologies. Deposition efficiency was increased with the increase of the hydrogen gas fraction as shown in the overall increases of the width and thickness of the single passed spraying beads. The increase of the deposition efficiency resulted from the increase of the gas enthalpy. Meanwhile, the increase of the symmetry of the spraying bead with the increase of the argon gas flow rate implies that the sharp depletion of the injected particles occurred during the flight. Figure 4 shows the phase compositions of the single passed spraying beads according to the plasma gas composition. As the argon gas flow rate was increased at the constant flow rate of the hydrogen gas, the phase fraction of the γ-Al_2O_3 to the α-Al_2O_3 was decreased. However, the hydrogen gas flow rate increased the γ-Al_2O_3 phase fraction. Because of the lower activation energy barrier of the γ-Al_2O_3 than α-Al_2O_3 phase, the liquid alumina

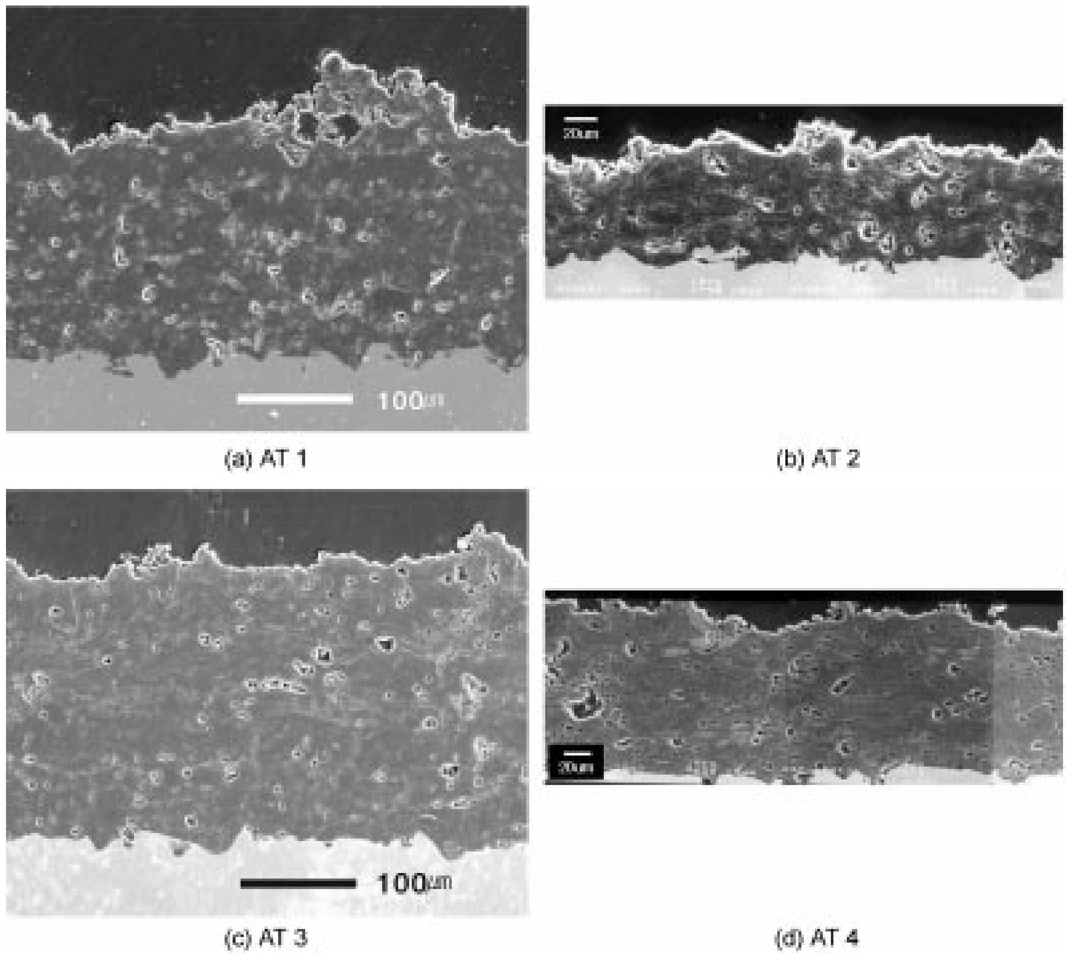

Fig. 5. Cross-sectional morphology of as-sprayed coatings according to the plasma gas compositions (See Table 1 for the plasma gas composition).

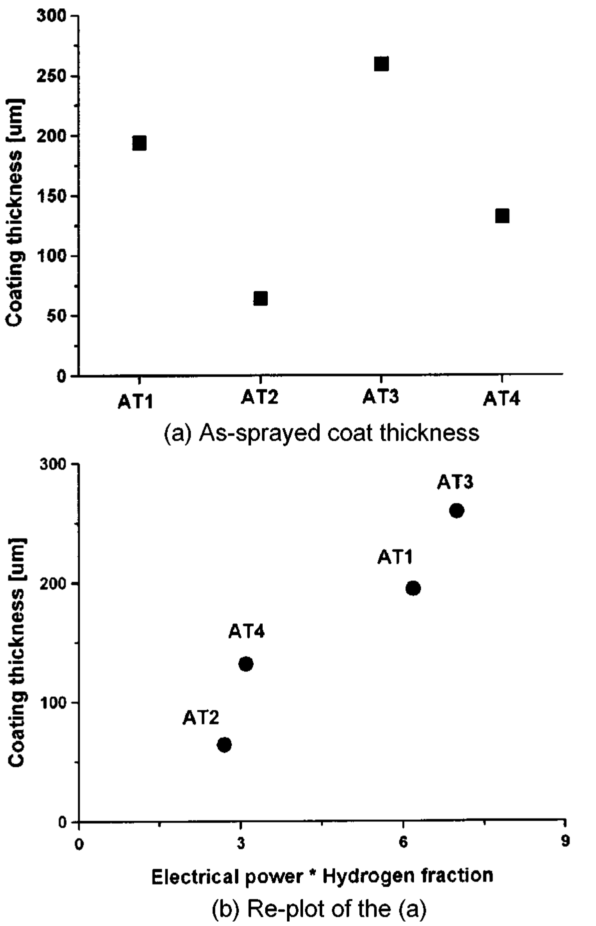

Fig. 6. Coating thickness according to the plasma gas composition (See Table 1 for the plasma gas composition).

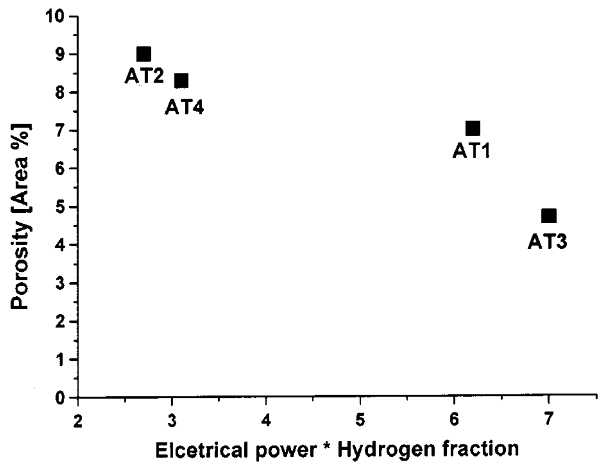

Fig. 7. Porosity according to the plasma gas composition (See Table 1 for the plasma gas composition).

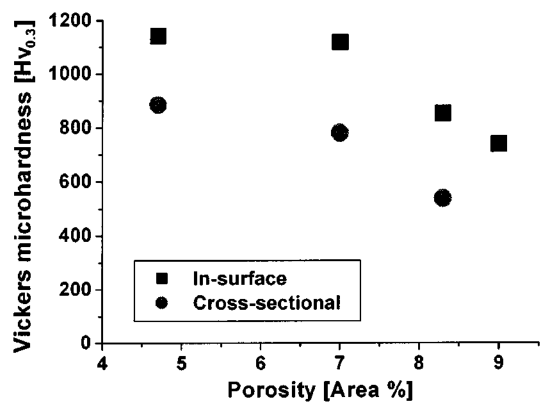

Fig. 8. Vickers microhardness according to the porosity.

phase solidifies to the γ-Al_2O_3 phase [6]. And it remains to the room temperature if the cooling rate is fast enough to prevent it from transforming to the α-Al_2O_3 phase. Therefore, the melting state of the impacting particle can be indirectly estimated through the γ-Al_2O_3 phase fraction in the spraying bead. However, the effects of the hydrogen gas and argon gas on the melting state of the impacting particles seemed to be different because both gases increased the spraying power. That is to say, the increase of the gas enthalpy with the increase of the hydrogen gas flow rate resulted in the increase of the melting state of the impacting particle. Meanwhile, the decrease of the melting degree with the increase of the argon gas flow rate resulted from the decrease of the residence time of the in-flight particle in the hot gas stream. The cross-sectional morphologies of the as-sprayed coatings are shown in Fig. 5. The alternate lamellar structures are observed; the bright field is rich in the titania while the gray field is rich in the alumina. The $H_{K\,0.05}$ value of the titania rich phase was 716 while that of the alumina rich phase was 944. This soft and hard phase mixture is considered to increase the fracture toughness. The thickness in the as-sprayed coatings according to the plasma gas composition is shown in Fig. 6(a). And the re-plot of the coating thickness against the multiplication of the electrical powder and the hydrogen gas fraction is present in the Fig. 6(b). The APS coating thickness seemed to have a linear relation with the newly suggested value. This might be due to the improvement of the melting state of the impacting particle with the increase of the spraying power and also the hydrogen gas flow rate. Coating porosity was also dependent on the melting state of the impacting particle as shown in Fig. 7. The porosity was linearly decreased with the increase of the gas enthalpy. Generally, the microhardness of the ceramic materials largely depends on the defect content and morphology. And thus, the microhardness of the APS coatings is also dependent on the porosity in the coating. It can be confirmed in Fig. 8; the plane view microhardness and the cross-sectional microhardness were increased with the decrease of the porosity resulting from the increase of the melting state of the impacting particles. Bond strength of the APS coatings shows the different characteristics. It shows closer relationship with the multiplied value of the electrical power and the argon gas flow rate as shown in Fig. 9. This might be due to the increase of the particle velocity according to the increase of the elec-

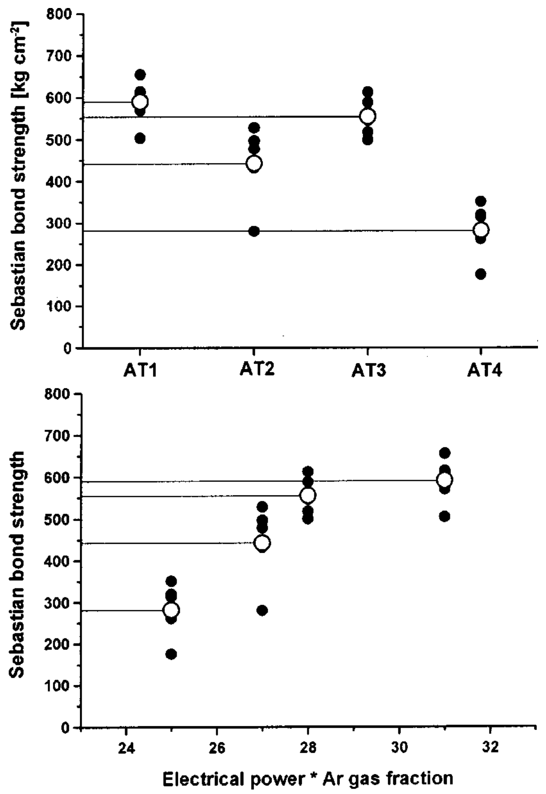

Fig. 9. Sebastian bond strength of Al_2O_3-TiO_2 coatings according to the plasma gas compositions (See Table 1 for the plasma gas composition).

Notation	AT1	AT2	AT3	AT4
Failure	Cohesive	Adhesive	Cohesive	Adhesive

trical power and the argon gas flow rate. The increased particle velocity results in the more intimate contact between the splat and splat, and splat and substrate [6, 7]. When the coatings were produced using the high hydrogen gas flow rate (20 FMR), the fractures occurred in the coating. But the adhesive fracture was observed at the low hydrogen gas flow rate (10 FMR). This is considered to be due to the substrate melting effect occurring at the high flow rate of the hydrogen gas. Figure 10 shows the phase fraction of the γ-Al_2O_3 to the α-Al_2O_3 of the as-sprayed coatings. And the effect of the additional heat input on the phase composition can be observed by comparing the phase composition of the single passed spraying bead. The APS coatings were deposited by overlaying the successive passes of a spraying bead. Therefore, the increased α-Al_2O_3 phase fractions in the coatings can be deduced by the additional heat treating effects of the successive passes; heat inputs through the plasma plume and hot molten droplets.

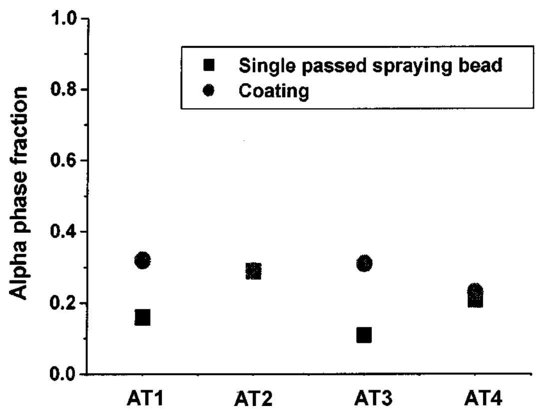

Fig. 10. Phase composition of the APS alumina-titania coating according to the plasma gas composition (See Table 1 for the plasma gas composition).

Conclusion

In this study, the effects of the plasma gas composition on the coating thickness, microhardness, and bond strength were observed. The flaw contents of coating decreased with the increase of the hydrogen volume fraction. This might be due to the increase of the melting state of an impacting particle and the resultant improvement in flattening. While kinetic energy as well as thermal energy of in-flight particles affected the bond strength of coating, the coating thickness and microhardness were dominantly dependent on the gas enthalpy.

Acknowledgement

The authors acknowledge that this study was supported by the CPRC (Ceramic Process Researching Center) in Hanyang university.

References

1. L. Pawlowski, in “The Science and Engineering of Thermal Spray Coatings” (John Wiley & Sons Ltd., 1995).
2. P. Fauchais and A. Vardelle, Int. J. of Therm. Sci. 39 (2000) 852-870.
3. S. Sampath and X. Jiang, Mater. Sci. and Eng. A 304/306 (2001) 144-150.
4. B. Liu, T. Zhang, and D.T. Gawne, Surf. and Coat. Tech. 132 (2000) 202.
5. J. Gong, J. Wu, and Z. Guan, J of the Euro. Cera. Soc. 19[15] (1999) 2625-2631.
6. R. McPherson, Thin Solid Films 83 (1981) 297.
7. S.P. Wang, G.X. Wang, and E.F. Matthys, Mat. Sci. and Eng. A262 (1999) 25.